SUPPORTING MATERIAL

Activation Thermodynamics of Poly(Ethylene Glycol)-Mediated Model Membrane Fusion Support Mechanistic Models of Stalk and Pore Formation

Hirak Chakraborty, Pradip K. Tarafdar, Michael J. Bruno, Tanusree Sengupta & Barry R. Lentz*

MATERIALS

Chloroform stock solutions of 1,2-dioleoyl-3-sn-phosphatidylcholine (DOPC), 1,2-dioleoyl-3-sn-phosphatidylethanolamine (DOPE), bovine sphingomyelin (SM) were purchased from Avanti Polar Lipids (Birmingham, AL) and used without further purification. The concentration of the stock lipids was determined by phosphate assay (1). Cholesterol was purchased from Avanti Polar Lipids and was further purified by published procedure (2). Hexadecane was purchased from Sigma Chemicals (St. Louis, MO). All other reagents were of the highest purity grade available.

METHODS

Vesicle Preparation:

Vesicles were prepared from a stock of DOPC/DOPE/SM/CH (molar ratio 35/30/15/20) in chloroform. Hexadecane was added to this mixture at a molar ratio of 3/100 hexadecane/total lipid for hexadecane-containing samples. Lipids at appropriate molar ratios in cyclohexane/methanol mixed solvent (1-2 drops of methanol in 1 ml of cyclohexane) were freeze dried under high vacuum overnight. Small, unilamellar vesicles (SUVs) were prepared as documented previously (3). The dried lipid powders were suspended in assay buffers for 1 hour above the phase transition temperature. The column and experimental buffer contained 100 mM NaCl, 1 mM EDTA, 1mM $CaCl_2$ and 10 mM MES, pH 5.0. All contents mixing, leakage and lipid mixing experiments were done at 0.2mM lipid.

ANTS/DPX contents mixing and leakage experiments:

Mixing and leakage of the trapped contents of sonicated, small, unilamellar vesicles (SUVs) composed of DOPC/DOPE/SM/CH (35/30/15/20 mol ratio %) lipids were monitored by the ANTS/DPX assay (4). For contents mixing, stock PEG solution was added to the ANTS and DPX-containing vesicle mixtures (1:1) and we measured the fluorescence quenching of the ANTS by DPX with time at 26^0 C. Fluorescence quenching of ANTS will only be observed if the contents of the ANTS-containing and DPX-containing vesicles mix with each other. For leakage experiments, stock PEG solution was added to vesicles containing ANTS/DPX, and we recorded the increase in fluorescence associated with dilution of these components into the external compartment and the associated loss of quenching. All experiments were done at pH 5.0.

Lipid Mixing Assay:

Fluorescent lipid probes with fluorophores attached to their acyl-chains, BODIPY500-PC and BODIPY530-PE (Molecular probes, Eugene, OR), were used for measuring lipid transfer during PEG- mediated vesicle fusion. In order to measure lipid transfer during PEG-mediated fusion, probe-containing vesicles were mixed with probe-free vesicles at a 1:4 ratio. PEG was added to the vesicle mixtures and changes in fluorescence intensity due to probe dilution were monitored with time. The emission intensities of donor and acceptor were recorded in T-format with channel A at 520 nm (slit 8 nm) and with a 550 nm cut off filter in channel B. Excitation was at 500 nm using slits of 4 nm. The ratio of donor/acceptor intensity was recorded as reflective of lipid mixing. The percent of lipid mixing was calculated using standard curves from measurements with vesicles containing different probe concentrations. It was assumed that 100% lipid mixing corresponded to a five-fold dilution of the probe. Details of this procedure are described in our earlier publications (5, 6).

Time Course Measurements:

Experiments were performed with 0.2 mM lipid incorporated into SUVs. Vesicles were equilibrated in a volume of 1.0 mL in a temperature-controlled cuvette for at least 10 minutes before addition of 1.0 mL of 10 wt% PEG in buffer (to yield 5 wt% PEG in the mixture) that had been equilibrated at the same temperature using a 1 mL Pipetteman syringe (Fisher Scientific) also maintained in temperature-equilibrated buffer. Experiments were performed using a Spex Fluorolog spectrofluorimeter (Jobin-Yvon, a division of Horiba, Inc). We forcefully injected the PEG solution into a cuvette containing vesicle sample and then withdrew and pushed the sample plus PEG into the cuvette at least three times. Data collection was begun at the time of PEG addition. Because we had to use manual mixing to insure complete mixing of PEG and buffer solutions, we miss 4-5 seconds, so fluorescence values were extrapolated to zero time using a two-exponential fit to the first 60 seconds of data. Adjusting the PEG concentration to near the threshold at which fusion occurs (5 wt %) reduced the rate of initial intermediate formation to a range measurable using manual mixing methods. The time constant for aggregation (judged by OD) was less than 3 s (more than 10 times faster than formation of the initial fusion intermediate), so aggregation was essentially complete by the time we began collecting data. Time courses for a given sample preparation were collected in triplicate and outliers were discarded. Data from at least three distinct samples were analyzed for each condition examined. Error in reported parameter values derive from averaging the parameters from these individual experiments. In addition, data from the independent experiments were sometimes combined and analyzed as a single data set. In these instances, parameter values were consistently inside the error range of the average values obtained from multiple determinations. This degree of care in obtaining and analyzing data sets was required in order to obtain parameter values of sufficiently low uncertainty for characterizing transition state thermodynamics. A caveat associated with our procedure is that we might miss processes that occur with characteristic times shorter than 4-5 s. The fastest lipid mixing we have ever observed ($\tau \sim 10$ s) was measured in a specially constructed rapid mixing syringe system (mixing time $\sim$ 1-2 s for 17.5 wt % PEG, much higher than used here) (7). Thus, under our conditions, we are likely not missing events faster than those reported here for initial lipid mixing.

Kinetic Model and Data Analysis:

Our kinetic model is based on the "modified stalk hypothesis" (8, 9), which proposes that individual fusion events proceed through two semi-stable non-lamellar structural intermediates to a final fusion pore. However, our experiments follow the behavior of ensembles of individual events (80 nM SUVs): roughly 50 million aggregated vesicles in an observation volume of ~ $1mm^3$ as they all proceed through these structural intermediates. Thus, the "states" in our kinetic model (10) are not structural states, but thermodynamic states consisting of a broad array of microstructures, each of which is roughly related to one of the structures associated with the modified stalk model. Early capacitance/conductance measurements on patch-clamped secretory cells demonstrated transitory or "flickering" capacitance steps occur early in the fusion process (11), while a "foot" of catecholamine release was detected just prior to final pore formation (12). While opening times derived from these electrical measurements are on the order of a millisecond, mean dwell times between early flickering events and final pores were much longer (many seconds) (13), consistent with our 2-intermediate model and with rate constants reported here and elsewhere (14). Observations on model membranes revealed similar behavior: early "flickering" pores occurred in the time frame of membrane lipid movement while a substantial but limited lipid "diaphragm" can be observed prior to final pore formation (15). More recent rapid single-vesicle measurements of lipid movement between SNARE-linked, protein-rich large, unilamellar vesicles (LUVs) also clearly resolve up to two, or maybe even three, intermediate states (16).

Based on these and many other observations, we modeled our data in terms of a sequential, 4-state (three-step) mechanism (see following Diagram), where each "state" is a thermodynamic ensemble of similar structural states or molecular arrangements ("microstructures")(10). While our observations (lipid mixing, content mixing, and content leakage) are macroscopically irreversible in the presence of PEG (7) (thus, the sequential treatment), the observation of "flickering" pores suggests that structures comprising each ensemble are likely microscopically reversible. In the accompanying diagram, 'nV' is a separated-vesicle state, 'A' represents vesicles in contact within aggregates, 'I_1' and 'I_2' are semi-stable intermediate states (presumably dominated by Stalk and ETMC microstructures, respectively), and 'FP' is the final **f**usion **p**ore state (FP).

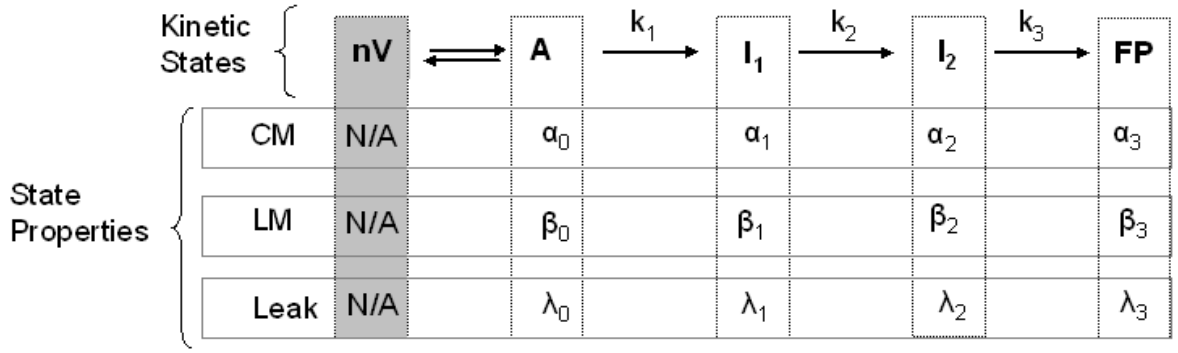

The rate constants for conversion between states are k_1, k_2 and k_3. Each state in the ensemble kinetic model is characterized by probabilities of lipid- (β_i's) and content-mixing (α_i's) and by a content leakage rate (λ_i}. The model can account for the time courses of five observables associated with PEG-mediated fusion (10), although the time courses of three

basic observables, lipid mixing (LM), contents mixing (CM), and leakage (L), are sufficient to uniquely define three rate constants that account for the other two observables (light scattering, and formation and disappearance of non-lamellar intermediates (17)) in all cases examined (5, 10). In addition to three rate constants, two adjustable probabilities and a leakage rate for each of the four states are required to describe the contribution of each state to a particular observable. While this might seem an excessive number of parameters, experimental observations allow for elimination of some of these. The probabilities of content and lipid mixing in the "A" state were negligibly small (*i.e.* $\alpha_0 = \beta_0 = 0$), and a very small amount of lipid mixing takes place in the FP state (β_3 is assumed to be close to zero). If leakage is significant in the FP state, this is obvious in the data (content mixing signal decreases at long time); otherwise λ_3 is taken as 0. Along with normalization conditions for the probabilities, this leads to three intrinsic rate constants and just five extensive parameters (six if λ_3 is needed) to describe three independent time courses that in most cases must be described by double exponentials. Although we have tried more complex (*e.g.*, parallel) models, in recording time courses for at least 15 experimental systems at multiple temperatures, we have yet to uncover a system in which the simple four-sequential-states model failed to account for the data in a physically reasonable way, although a simpler (three-intermediate) model was at times appropriate. Of course interpretation of the temperature dependence of equilibrium or kinetic processes (see next section) is always dependent on the appropriateness of the assumed model. While we argue that our model is reasonable and can account for all data we have collected on a variety of fusing systems, it could of course be an over simplification of the real process. With this caveat and within current knowledge of the fusion mechanism, we feel that the approach employed here offers new experimental insights into the fusion process.

Calculation of Transition State Thermodynamics:

If initial and transition states for a process are in equilibrium, Eyring's transition state theory can yield information about the thermodynamics of the transition state relative to the initial state. We calculated the activation free energy of each step (ΔG_i^*) using the equations, $k_i = A\mathrm{e}^{-\Delta G_i^*/k_B T}; \Delta G_i^* = -k_B T \ln(\frac{k_i}{A})$, where k_i's are the rate constants of different steps and "A" is a pre-exponential factor that contains both the classical "transmission factor" (κ) and a fixed frequency (ν) at which transition state microstructures are assumed to decay to product structure.

Eyring's term for this decay frequency ($k_B T/h$) is appropriate only to a simple bimolecular gas-phase collisional reaction in which the reaction coordinate corresponds to a weak vibrational motion along the collision axis. In this case, the partition functions for the initial and transition states are assumed to differ in only this motion, resulting in the traditional Eyring expression. Fusion is a much more complex process in which the partition functions for the initial and transition states differ not in a single motion but according to the ensembles of molecular structures contributing to these "states". Chan and Dill make a similar argument in discussing another complex process involving multiple intermediate "states", namely protein folding, for which each state requires a multi-dimensional configurational space (18). Similarly, in membrane fusion, multiple lipid and water molecules must rearrange to accomplish certain steps. Since we cannot assign the

transition state to a simple motion of a single atom, we arbitrarily assumed a temperature-independent value for A of 1 s^{-1}. This has two consequences. First, it assumes that the T-dependence of k_i is assigned solely to the T-dependence of ΔG_i^*. For a complex process such as fusion, this is a necessary and acceptable assumption. Second, it establishes an arbitrary y-intercept for ΔG_i^*. A cubic equation was found to be the simplest polynomial that would adequately describe the variation of ΔG_i^* with temperature for experiments performed on a wide variety of fusing vesicle systems. While the activation free energy has an arbitrary magnitude, changes in activation free energy ($\Delta\Delta G_i^*$), are defined in units dependent on the value of k_B (here in kcal/mol). Activation entropy (ΔS^*) was calculated using the expression, $\Delta S^* = -[\frac{\delta(\Delta G^*)}{\delta T}]_P$, leading to $\Delta H^* = \Delta G^* + T\Delta S^*$, with these quantities also having arbitrary magnitudes. However, the activation heat capacity ($\Delta C_p^* = (\frac{\partial \Delta H^*}{\partial T})_P$) does not depend on the arbitrary value of A.

The Modified Stalk Model of Fusion Intermediate Structures

The free energy profile (Figure S1) for the transition between stalk (I_1) and I_2 structures through a transition state (TS2) derives from a published calculation of fusion intermediate free energies as a function of increasing "stalk radius" (r_S shown in the "dimpled stalk" geometry in Figure S1) (19). The stalk radius is defined as zero when the hydrophobic surfaces of merged *cis* leaflets first touch (Figure S1). In this calculation, the detailed geometry at each stalk radius was adjusted to minimize energy (19). State A occurs when two bilayers are brought into "contact", which corresponds to a phosphate-phosphate distance of ~ 5Å (20). All free energies in Figure S1 are relative to this state, which has considerable curvature stress due to positively curved outer (*cis,* or contacting) leaflets and negatively curved inner (*trans*, or non-contacting) leaflets. The energy trajectory for the process examined by these bulk property calculations is akin to a linear "configurational space" whose curvature will dictate configurational entropy that contributes to the probability of observing any state along the reaction diagram. Obviously, variation in other geometric parameters will also contribute to the configurational entropy, but minimizing the energy at each stalk radius with respect to these parameters removes this complication and focuses on the assumed fusion trajectory (stalk radius).

The calculated energy along this path is dominated by three "Bulk Material" contributions: bending energy, interstice energy, and "compression/expansion energy" (19). The bending energy results from a mismatch between the mechanical curvatures of the structure and the "intrinsic curvatures" or shapes of the molecules comprising the bilayer. The "compression/expansion energy" results from the fact that the areas of the bilayer's two leaflets are different in the original unfused vesicles, creating a free energy component that opposes expansion unless lipids redistribute between leaflets (19). Because neutral lipids do redistribute during PEG-mediated fusion of SUVs (21), this energy is negligible, meaning that bending and interstice free energies dominate the hypothetical reaction diagram in Figure S1. Our results are formulated in terms of enthalpy or entropy differences between intermediate or transition states. In order to compare our

results to predictions of the "Bulk Materials" model, we must consider the possible microscopic origins of bending and interstice energies and the thermodynamic consequences of these. Bending energy derives from mismatch between lipid intrinsic curvature and geometric curvature and contains both enthalpic and entropic terms. To a rough approximation, we assign positive curvature stress largely to entropically unfavorable water-hydrocarbon interactions and negative curvature stress largely to loss of enthalpically favorable chain-chain interactions and gain in enthalpically unfavorable headgroup-headgroup interactions. The "interstice energy" results from packing inconsistencies between the lamellar and non-lamellar parts of a structure (shaded areas noted by arrows in Figure S1) (19, 22). Because reducing these packing inconsistencies requires water-hydrocarbon contact as well as lipid tilting and acyl chain splaying, the "interstice energy" also has both enthalpic ("void") and entropic (increasing water-hydrocarbon contact needed to reduce void) components. While clearly over simplified, a more detailed attempt to breakdown bending and interstice energies into thermodynamic quantities would be inappropriate. These assignments are particularly important in interpreting the effects of hexadecane on Step 2, as summarized in Figure S2.

EFFECTS OF HEXADECANE ARE CONSISTENT WITH PROPOSED MODELS

While hexadecane had little effects on rates (except perhaps for pore formation, k_3), it had significant effects on activation thermodynamics and on the probabilities of transient pore formation. The effects of hexadecane on the activation thermodynamics of all three steps are illustrated in Figures 2 and 4. We ask whether its effects are consistent with the models of these steps introduced here: Chain Protrusion, Bulk Materials, and Correlated Lipid Movement. For Step 1, the Acyl Chain Protrusion model predicts that TS1 already has a good deal of water-hydrocarbon interaction and significant configurational entropy, so adding hexadecane should do little to increase water-hydrocarbon contact or configurational entropy. Its effects on A state may well be greater. In general, it should occupy hydrophobic space near the ends of acyl chains and increase the area per head group in A state, thus increasing water-hydrocarbon contact. Replacing water-water and water-headgroup interactions with water-hydrocarbon interaction will increase A state enthalpy and configurational entropy, *i.e.*, make "A state" a bit more like the TS1, explaining the negative $\Delta\Delta H_1^*$ and $T\Delta\Delta S_1^*$ (Figure 4A). Both become more negative with increasing temperature. Hexadecane's effects should increase as the acyl chain and hexadecane configurational freedom increases, so its effects should increase with temperature as well. Consistent with this, $\Delta\Delta Cp_1^*$ is negative and becomes more so with temperature (Figure 4A).

In order to examine hexadecane's effect on k_2, we turn to the "Bulk Materials Model" (19). In doing so, we first note that hexadecane alters fusion intermediates in two distinct ways. First, hydrocarbons partition into both the interstice and acyl chain regions of hexagonal phases, but prefer the interstice space as hydrocarbon chain length increases (23). It is reasonable to assume that hexadecane could occupy both regions in fusion intermediates depending on both its conformation and lipid acyl chain conformation. In this way, it should influence mainly interstice energy but, depending on circumstances, should be able to alter bending energy as well. Second, to the extent that it occupies

interstice space and lowers interstice energy, it is predicted to alter the geometry and energy profiles of the I_1 state and TS2 (19). The multiple possible effects of hexadecane make it difficult to determine conclusively whether the "Bulk Materials Model" is consistent with our observations. The arguments in support of this require that hexadecane-triggered changes in bending and interstice energy be interpreted in terms of thermodynamic quantities, as outlined in the previous section, and that the influence of hexadecane's interstice filling ability on TMC and ETMC geometries is taken into account. This interpretation derives from predictions of how intermediate geometry depends on interstice energy, as documented in Figures 3 and 4 of reference (19). Figure S2 was constructed based on these published calculations and summarizes *rough magnitudes* of the effects expected from hexadecane's effects on interstice energy, bending energy, and geometry in SUVs. Even though hexadecane is commonly expected mainly to occupy "void" and reduce interstice energy (22), it is not fixed in one region of a lamellar or non-lamellar structure and affects several aspects of I_1 state or TS2 structure (23). For this reason, the effects illustrated in Figure S2 are organized and labeled according to whether they derive from the ability of hexadecane to align with acyl chains and alter bending energy (α) or occupy interstice (void) volume (β). These effects should produce both a shift in intermediate geometry (stalk radius increases) and a change in energy profile curvature for I_1, I_2, and TS2 structures (see Figure 4B of reference (19)). We used Figure 3B of reference (19) to assign the results of geometry shifts to changes in bending or interstice energies, and then the reasoning described above to derive the shifts in enthalpy and entropy illustrated in Figure S2. The different terms from Figure S2 contribute to the net change in transition state enthalpy due to adding hexadecane according to:

$$\begin{aligned}\Delta\Delta H_2^* &= (H_{TS2,hex} - H_{S,hex}) - (H_{TS2} - H_S) \\ &= H_{TS2,hex} - H_{TS2} - (H_{S,hex} - H_S) \\ &= \Delta\Delta H_{b\alpha} + \Delta\Delta H_{b\beta} + \Delta\Delta H_{V\beta} = \Delta\Delta H_\alpha + \Delta\Delta H_\beta\end{aligned}$$

A similar equation obtains for $-T\Delta\Delta S_2^*$. The effects of both chain-aligned and interstice-filling conformations contribute to the significant negative $\Delta\Delta H_2^*$ observed at low temperature (Figure S1B). The origin of the observed large negative $T\Delta\Delta S_2^*$ is more difficult to explain and thus more uncertain. Hexadecane-induced geometry shift produces a positive contribution from interstice energy but a somewhat larger negative contribution from bending energy, so these effects largely cancel (perhaps a small net negative contribution attributed to increased water-hydrocarbon contact in TS2). Bending energy makes a small negative contribution (attributed to water-hydrocarbon contact in I_1). Finally the curvature-reducing effect of reduced interstice energy provides a small negative shift in conformational entropy (Figure S2).

As temperature increases, the chain-aligned configuration of hexadecane should become less probable in favor of the "void-filling" configuration. The result would be a loss in the negative bending energy contributions to $T\Delta\Delta S_2^*$ but an increase in the small net negative contribution from hexadecane-induced geometry shift, producing the less dramatically negative $T\Delta\Delta S_2^*$ observed at high temperature. The shift in $\Delta\Delta Cp_2^*$ from

negative to positive also reflects hexadecane-induced water ordering in TS2 as temperature increases (see $-TS_{H\Phi v\beta}$ *versus* $-TS_{H\Phi b\beta}$ in Figure S2). Finally, the increasing contribution of hexadecane-induced stalk configurational entropy at high temperature stabilizes I_1 relative to TS2 with increasing temperature (k_2 in Table S2). If the reader accepts these arguments, hexadecane alters Step 2 in a way consistent with predictions based on the published Bulk Materials model (19).

For Step 3, in contrast to Steps 1 and 2, hexadecane increased both ΔH_3^* and $T\Delta S_3^*$ and reduced ΔCp_3^* at all temperatures (Figure 4C). As noted, hexadecane can alter both the energy and geometry of the I_2 or TS3 structures. We argue that its effects on geometry are most important in interpreting our observations. Since $\Delta\Delta Cp_3^*$ is negative, hexadecane must have increased water exposure to hydrocarbon in I_2 more than in TS3, or decreased it in TS3 more than in I_2. The ability of hexadecane to reduce interstice energy will shift the I_2 state energy minimum to larger r_S, where diaphragm expansion will increase the circumferential negative curvature of merged *cis* leaflets. This should increase the number of enthalpically unfavorable microstructures contributing to I_2. The TS3 ensemble will be similarly affected, except that it involves correlated rearrangements of larger numbers of lipid molecules, which will be even more enthalpically unfavorable. The net results should be a positive $\Delta\Delta H_3^*$, as observed (Figure S2). In the absence of hexadecane, we suggested that a difference in configurational entropy between these two states produced a positive $T\Delta S_3^*$. An increase in r_S should increase the number of microstates contributing to both I_2 and TS3 and thus increase this difference in configurational entropy, consistent with the observed positive $T\Delta\Delta S_3^*$. ΔCp_3^* in the absence of hexadecane is negative (Figure 3C) and hexadecane makes it more negative (Figure 4C inset). We interpreted the negative ΔCp_3^* as reflecting a difference in thermal heat capacity. If we view the principle effect of hexadecane as increasing r_S at which I_2 exists, it should increase the thermal heat capacity of TS3 as well as the difference between the thermal heat capacities of I_2 and TS3. Thus, it can be reasonably argued that the influence of hexadecane on I_2 and TS3 geometry can account for its influence on Step 3 transition thermodynamics.

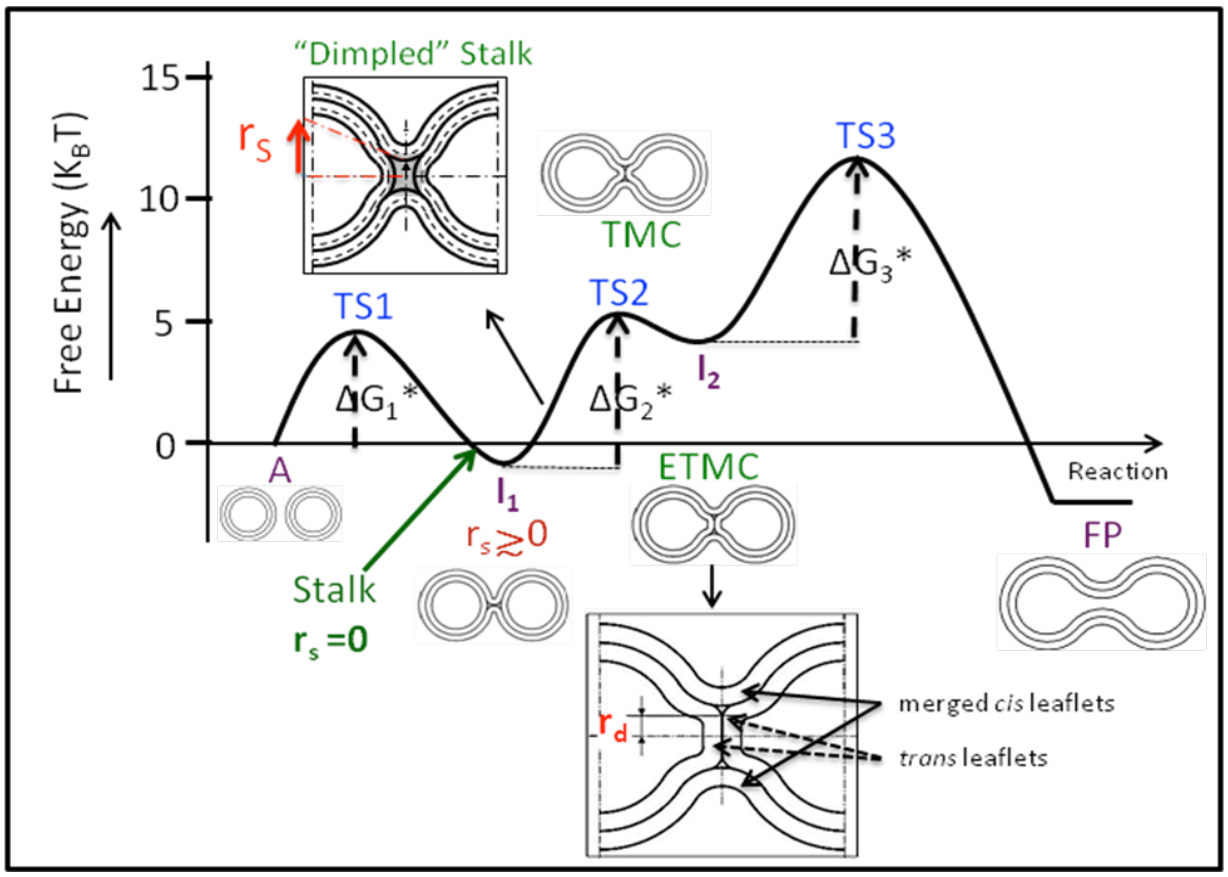

Figure S1: Schematic representation of the fusion reaction profile for PEG-mediated fusion of PC/PE/SM/CH SUVs derived from our results at 26°C. Geomteries mentioned in the text are labeled in green. Reaction states are labbled in purple. Transition states are labeled in blue. The "reaction coordinate" for this diagram is the "stalk radius" (r_s) that is illustrated in the "dimpled stalk" diagram and is defined as "0" when the two merged *trans*- leaflets touch. Estimates of ΔG_1^* and ΔG_3^* were obtained from the rate constants determined in this study. The path from (I_1 to I_2) is based on a published calculation that used a lipid composition different from the one used here (19), so ΔG_2^* was also adjusted to match our measured k_2. Nonetheless, the key features of the reaction free energy diagram are independent of composition, although their details (*e.g.*, stalk radii corresponding to I_1, TMC, or I_2) will vary with composition (19). The geometries shown for intermediate structures derive from minimization of the free energies of structures at fixed stalk radii (19).

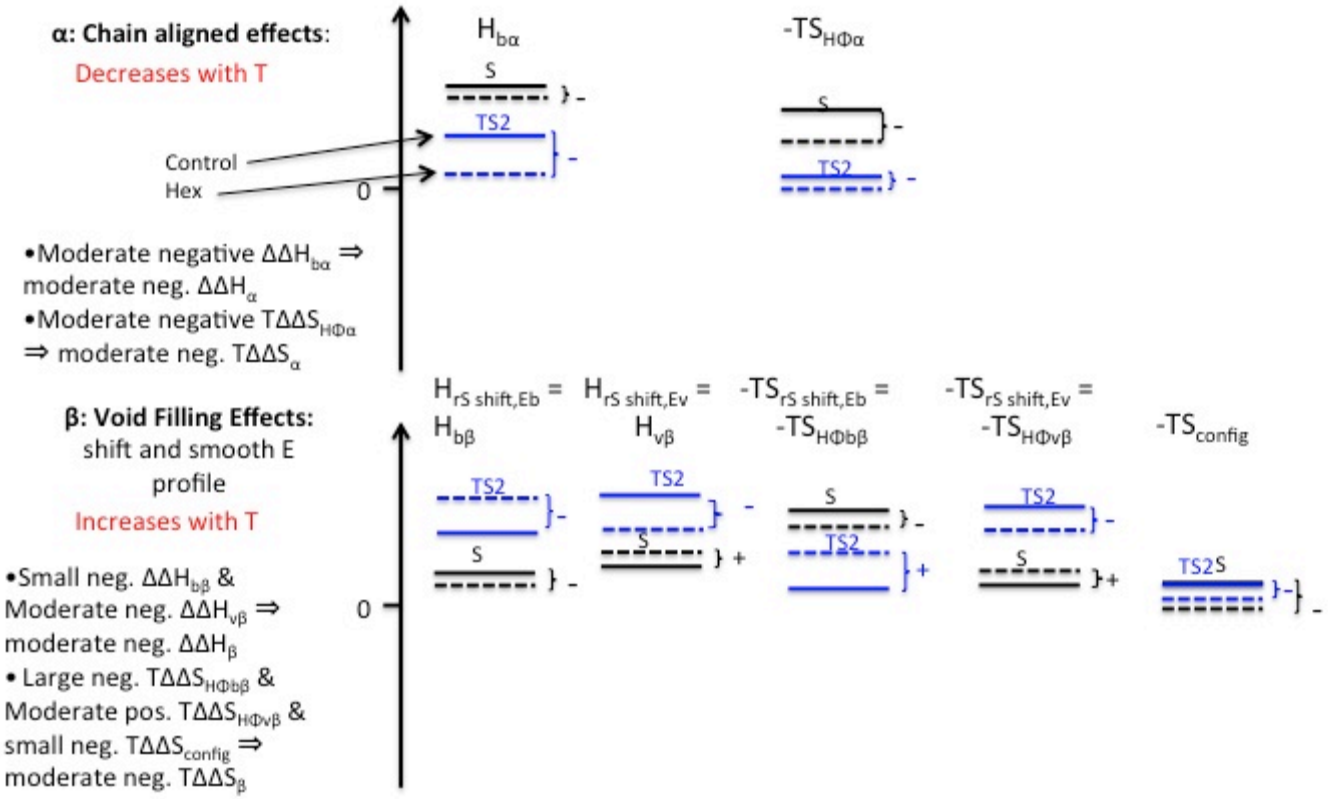

Figure S2: Effects of hexadecane on Step 2. Cartoon illustrates the rough magnitudes of changes (arbitrary units) in bending energy (H_b), void energy (H_v), hydrophobic entropy ($TS_{H\Phi}$), and configurational entropy (TS_{cofig}) for stalk (S) and the second transition state (TS2) associated with addition of hexadecane to SUVs. The changes are illustrated by the distance between values estimated for control (solid lines) *versus* hexadecane-containing (dashed lines) vesicles.

Table-S1. Rate constants and probabilities of intermediate states for control vesicles.

Parameters were obtained by fitting lipid mixing, content mixing, and content leakage time courses to a sequential two-intermediate model as described in the text. All the experiments were performed at least three times, with analysis carried out on the combined time courses. The errors presented in the Table are the parameter uncertainties from this combined analysis, although parameters from analysis of all experiments normally fell within this range of uncertainty.

				Contents mixing				Lipid mixing			Leakage		
Temp (^{0}C)	k_1 x 10^3 (s^{-1})	k_2 x 10^3 (s^{-1})	k_3 x 10^3 (s^{-1})	α_1 (I_1)	α_2 (I_2)	α_3 (FP)	f_{CM}	β_1 (I_1)	β_2 (I_2)	f_{LM}	λ_0 x 10^4 (s^{-1}) (I_0)	λ_1 x 10^4 (s^{-1}) (I_1)	λ_2 x 10^4 (s^{-1}) (I_2)
26	11.4± 0.56	2.71± 0.12	0.86± 0.09	0.12± 0.01	0.35± 0.03	0.53± 0.04	0.15	0.54± 0.07	0.46± 0.06	0.45	0.57±0.02	0.33±0.01	0.35±0.01
30	12.2± 0.59	3.52± 0.17	1.03± 0.02	0.38± 0.01	0.20± 0.01	0.42± 0.02	0.21	0.63± 0.09	0.37± 0.06	0.48	0.96±0.06	0.94±0.04	0.44±0.02
34	16.6± 0.68	4.90± 0.21	1.25± 0.01	0.38± 0.01	0.20± 0.01	0.42± 0.02	0.24	0.69± 0.08	0.31± 0.04	0.46	2.19±0.07	1.91±0.04	0.78±0.01
38	20.2± 0.71	5.66± 0.31	1.42± 0.02	0.40± 0.01	0.20± 0.01	0.38± 0.02	0.27	0.77± 0.08	0.23± 0.02	0.48	4.09±0.13	2.98±0.07	0.95±0.02
43	25.7± 0.75	7.07± 0.29	1.52± 0.02	0.44± 0.01	0.20± 0.01	0.36± 0.02	0.29	0.77± 0.07	0.23± 0.02	0.46	5.79±0.15	5.20±0.07	1.97±0.02

Table-S2. Rate constants and probabilities of intermediate states for control vesicles containing 3mol% hexadecane.

Parameters were obtained by fitting lipid mixing, content mixing, and content leakage time courses to a sequential two-intermediate model as described in the text. All the experiments were performed at least three times, with analysis carried out on the combined time courses. The errors presented in the Table are the parameter uncertainties from this combined analysis, although parameters from analysis of all experiments normally fell within this range of uncertainty.

				Contents mixing				Lipid mixing			Leakage		
Temp (^{0}C)	k_1 x 10^3 (s^{-1})	k_2 x 10^3 (s^{-1})	k_3 x 10^3 (s^{-1})	α_1 (I_1)	α_2 (I_2)	α_3 (FP)	f_{CM}	β_1 (I_1)	β_2 (I_2)	f_{LM}	λ_0 x 10^4 (s^{-1}) (I_0)	λ_1 x 10^4 (s^{-1}) (I_1)	λ_2 x 10^4 (s^{-1}) (I_2)
26	14.4± 0.70	2.71± 0.01	0.72± 0.01	0.39± 0.01	0.35± 0.01	0.26± 0.02	0.46	0.54± 0.06	0.46± 0.05	0.51	2.32±0.01	1.58±0.01	0.39±0.01
30	15.7± 0.58	3.04± 0.14	2.05± 0.01	0.54± 0.03	0.18± 0.01	0.28± 0.04	0.48	0.61± 0.06	0.39± 0.04	0.50	4.19±0.11	1.95±0.01	0.58±0.01
34	18.6± 0.63	3.81± 0.15	2.82± 0.08	0.61± 0.03	0.14± 0.01	0.25± 0.04	0.52	0.66± 0.06	0.34± 0.03	0.53	8.72±0.23	3.34±0.12	1.05±0.01
38	20.9± 0.63	4.15± 0.19	3.96± 0.14	0.68± 0.04	0.13± 0.01	0.19± 0.05	0.49	0.73± 0.06	0.27± 0.02	0.51	13.03±0.38	4.02±0.20	1.38±0.17
43	22.9± 0.86	4.93± 0.27	4.21± 0.01	0.65± 0.01	0.17± 0.01	0.18± 0.02	0.51	0.75± 0.05	0.25± 0.02	0.50	25.94±0.57	5.78±0.20	1.02±0.01

Table S3: Parameters obtained by fitting the plot of ΔG_i^* vs. temperature (Figure 2) using the equation $\Delta G_i^*(kcal/mol) = y_{0,i} + a_i T + b_i T^2 + c_i T^3$ for the fusion of control vesicles and the vesicles in presence of 3 mol% hexadecane. The same parameters were used to obtain $T\Delta S_i^*$ ($-a_i T - 2b_i T^2 - 3c_i T^3$); ΔH_i^* ($y_{0,i} - b_i T^2 - 2c_i T^3$), and ΔCp_i^* ($-2b_i T - 6c_i T^2$) in Figure 3 and Figure 4.

		y_{0i}	a_i	b_i	c_i
Control	First step	-1665 ± 62	16.2 ± 1.1	$-5.26\times10^{-2} \pm 0.37\times10^{-2}$	$5.68\times10^{-5} \pm 0.40\times10^{-5}$
	Second step	-188.2 ± 3.54	2.16 ± 0.35	$-7.89\times10^{-3} \pm 1.12\times10^{-4}$	$9.396\times10^{-6} \pm 1.22\times10^{-7}$
	Third step	-742 ± 12	7.46 ± 0.54	$-2.48\times10^{-2} \pm 0.17\times10^{-2}$	$2.74\times10^{-5} \pm 0.16\times10^{-5}$
3 mol% hexadecane	First step	-2458 ± 128	23.9 ± 1.2	$-7.81\times10^{-2} \pm 0.04\times10^{-2}$	$8.49\times10^{-5} \pm 0.44\times10^{-5}$
	Second step	582 ± 11	-5.53 ± 0.27	$1.74\times10^{-2} \pm 5.52\times10^{-4}$	$-1.82\times10^{-5} \pm 0.04\times10^{-5}$
	Third step	1384 ± 174	-12.7 ± 1.7	$3.91\times10^{-2} \pm 0.20\times10^{-3}$	$-4.0\times10^{-5} \pm 0.2\times10^{-5}$

References:

1. Chen, P. S., T. Y. Toribara, and H. Warner. 1956. Microdetermination of Phosphorus. Anal Chem 28:1756-1758.
2. Haque, M. E., T. J. McIntosh, and B. R. Lentz. 2001. Influence of lipid composition on physical properties and peg-mediated fusion of curved and uncurved model membrane vesicles: "nature's own" fusogenic lipid bilayer. Biochemistry 40:4340-4348.
3. Lentz, B. R., T. J. Carpenter, and D. R. Alford. 1987. Spontaneous fusion of phosphatidylcholine small unilamellar vesicles in the fluid phase. Biochemistry 26:5389-5397.
4. Haque, M. E., A. J. McCoy, J. Glenn, J. Lee, and B. R. Lentz. 2001. Effects of hemagglutinin fusion peptide on poly(ethylene glycol)-mediated fusion of phosphatidylcholine vesicles. Biochemistry 40:14243-14251.
5. Haque, M. E., H. Chakraborty, T. Koklic, H. Komatsu, P. H. Axelsen, and B. R. Lentz. 2011. Hemagglutinin Fusion Peptide Mutants in Model Membranes: Structural Properties, Membrane Physical Properties, and PEG-Mediated Fusion. Biophysical Journal 101:1095-1104.
6. Malinin, V. S., M. E. Haque, and B. R. Lentz. 2001. The rate of lipid transfer during fusion depends on the structure of fluorescent lipid probes: a new chain-labeled lipid transfer probe pair. Biochemistry 40:8292-8299.
7. Lee, J., and B. R. Lentz. 1997. Evolution of lipidic structures during model membrane fusion and the relation of this process to cell membrane fusion. Biochemistry 36:6251-6259.
8. Kozlov, M. M., S. L. Leikin, L. V. Chernomordik, V. S. Markin, and Y. A. Chizmadzhev. 1989. Stalk mechanism of vesicle fusion. Intermixing of aqueous contents. European Biophysics Journal 17:121-129.
9. Siegel, D. P. 1999. The modified stalk mechanism of Lamellar/Inverted phase transitions and its implications for membrane fusion. Biophys J 76:291-313.
10. Weinreb, G., and B. R. Lentz. 2007. Analysis of membrane fusion as a two-state sequential process: evaluation of the stalk model. Biophys J 92:4012-4029.
11. Fernandez, J. M., E. Neher, and B. D. Gomperts. 1984. Capacitance measurements reveal stepwise fusion events in degranulating mast cells. Nature 312:453-455.
12. Chow, R. H., L. von Ruden, and E. Neher. 1992. Delay in vesicle fusion revealed by electrochemical monitoring of single secretory events in adrenal chromaffin cells. Nature 356:60-63/Users/uncbrl/Documents/Barry's Files/PDFlibrary/Fusion/Neher foot.pdf.
13. Oberhauser, A. F., J. R. Monck, and J. M. Fernandez. 1992. Events leading to the opening and closing of the exocytotic fusion pore have markedly different temperature dependencies. Kinetic analysis of single fusion events in patch-clamped mouse mast cells. Biophysical Journal 61:800-809.
14. Lee, J., and B. R. Lentz. 1998. Secretory and viral fusion may share mechanistic events with fusion between curved lipid bilayers. Proc Natl Acad Sci U S A 95:9274-9279.
15. Chanturiya, A., L. V. Chernomordik, and J. Zimmerberg. 1997. Flickering fusion pores comparable with initial exocytotic pores occur in protein-free phospholipid bilayers.

Proceedings of the National Academy of Sciences of the United States of America 94:14423-14428.
16. Yoon, T.-Y., B. Okumus, F. Zhang, Y.-K. Shin, and T. Ha. 2006. Multiple intermediates in SNARE-induced membrane fusion. Proceedings of the National Academy of Sciences of the United States of America 103:19731-19736.
17. Malinin, V. S., and B. R. Lentz. 2002. Pyrene Cholesterol Reports the Transient Appearance of Nonlamellar Intermediate Structures during Fusion of Model Membranes. Biochemistry 41:5913-5919.
18. Chan, H. S., and K. A. Dill. 1998. Protein folding in the landscape perspective: Chevron plots and non-Arrhenius kinetics. Proteins 30:2-33.
19. Malinin, V. S., and B. R. Lentz. 2004. Energetics of vesicle fusion intermediates: comparison of calculations with observed effects of osmotic and curvature stresses. Biophys J 86:2951-2964.
20. Burgess, S. W., T. J. McIntosh, and B. R. Lentz. 1992. Modulation of poly(ethylene glycol)-induced fusion by membrane hydration: importance of interbilayer separation. Biochemistry 31:2653-2661.
21. Lentz, B. R., W. Talbot, J. Lee, and L. X. Zheng. 1997. Transbilayer lipid redistribution accompanies poly(ethylene glycol) treatment of model membranes but is not induced by fusion. Biochemistry 36:2076-2083.
22. Rand, R. P., N. L. Fuller, S. M. Gruner, and V. A. Parsegian. 1990. Membrane curvature, lipid segregation, and structural transitions for phospholipids under dual-solvent stress. Biochemistry 29:76-87.
23. Chen, Z., and R. P. Rand. 1998. Comparative study of the effects of several n-alkanes on phospholipid hexagonal phases. Biophysical Journal 74:944-952.